

Original Article

Renewal and Differentiation of GCD Necklace Olfactory Sensory Neurons

Maria Lissitsyna Bloom, Lucille B. Johnston, and Sandeep Robert Datta[®]

Department of Neurobiology, Harvard Medical School, Boston, MA 02115, USA

Correspondence to be sent to: Sandeep Robert Datta, Department of Neurobiology, Harvard Medical School, Goldenson Building Room 420, 200 Longwood Ave, Boston, MA 02115, USA. e-mail: srdatta@hms.harvard.edu

Editorial Decision 17 April 2020.

Abstract

Both canonical olfactory sensory neurons (OSNs) and sensory neurons belonging to the guanylate cyclase D (GCD) “necklace” subsystem are housed in the main olfactory epithelium, which is continuously bombarded by toxins, pathogens, and debris from the outside world. Canonical OSNs address this challenge, in part, by undergoing renewal through neurogenesis; however, it is not clear whether GCD OSNs also continuously regenerate and, if so, whether newborn GCD precursors follow a similar developmental trajectory to that taken by canonical OSNs. Here, we demonstrate that GCD OSNs are born throughout adulthood and can persist in the epithelium for several months. Phosphodiesterase 2A is upregulated early in the differentiation process, followed by the sequential downregulation of β -tubulin and the upregulation of CART protein. The GCD and MS4A receptors that confer sensory responses upon GCD neurons are initially expressed midway through this process but become most highly expressed once CART levels are maximal late in GCD OSN development. GCD OSN maturation is accompanied by a horizontal migration of neurons toward the central, curved portions of the cul-de-sac regions where necklace cells are concentrated. These findings demonstrate that—like their canonical counterparts—GCD OSNs undergo continuous renewal and define a GCD-specific developmental trajectory linking neurogenesis, maturation, and migration.

Key words: adult neurogenesis, guanylate cyclase D, main olfactory epithelium, MS4A, necklace olfactory system, neuronal migration, neuronal regeneration

Introduction

Mice detect and encode odor chemical messages through several parallel olfactory circuits. These olfactory subsystems are built from distinct populations of olfactory sensory neurons (OSNs) that each express a specialized receptor repertoire and exhibit different patterns of anatomical connectivity with downstream circuits (Luo, 2008; Munger, 2009; DeMaria and Ngai, 2010; Uchida et al., 2014; Liberles, 2015; Ma et al., 2015; Mohrhardt et al., 2018). These molecular and anatomical differences endow each olfactory subsystem with a unique functional role in detecting and encoding olfactory stimuli and in driving appropriate behavioral responses to odors.

The best understood of these subsystems, the main olfactory system, is a generalist—its constituent sensory neurons express

a large family of broadly tuned odorant receptors (ORs) capable of interacting with diverse odors in the environment (Axel, 1995). Information from this main system is distributed across the paleocortical mantle to support odor discrimination, generalization, and learning. In contrast, sensory neurons of the guanylate cyclase D (GCD) “necklace” subsystem express the transmembrane receptor GCD, as well as a handful of receptors belonging to the *Ms4a* gene family; this receptor complement enables the GCD system to specifically interact with volatiles and gases such as carbon disulfide and carbon dioxide, peptides including uroguanylin and guanylin, and a specific subset of food-, conspecific-, and predator-derived odorants (Lin et al., 2004; Hu et al., 2007; Leinders-Zufall et al., 2007; Gao et al., 2010; Munger et al., 2010; Greer et al., 2016). Although the

central targets of the GCD subsystem remain unclear, it is thought to play a privileged role in a specific form of social odor learning (Munger et al., 2010; Arakawa et al., 2013).

Nearly all olfactory epithelia sit at an air or water interface, rendering their sensory neurons uniquely susceptible to environmental insults. The olfactory system is thought to address this challenge by replacing sensory neurons as they become aged or damaged by debris, toxins, and common pathogens (such as *Adenovirus*, *Streptococcus*, and *Staphylococcus* spp.) (Hinds et al., 1984; Seiden, 2004; Vent et al., 2004; Kondo et al., 2009; Brook, 2011; Ajmani et al., 2016; Imamura and Hasegawa-Ishii, 2016). This model is supported by the observation that mice raised in a pathogen-free environment have longer-lived OSNs than normally housed animals (Hinds et al., 1984) and that the rate of neurogenesis is highest in the anterior main olfactory epithelium (OE), which presumably encounters drier and “dirtier” air than more posterior regions (Weiler and Farbman, 1998a).

The molecular and cellular processes that govern ongoing renewal have been best characterized for the canonical OSNs that make up the main olfactory system. Globose basal cells (GBCs) act as primary olfactory stem cells, with the daughters of GBCs undergoing multiple differentiation steps before becoming immature OSNs (Schwob et al., 2017; Sokpor et al., 2018). After their final mitosis, immature OSNs express high levels of β -tubulin III (TUBB3/TUJ1) and growth-associated protein 43 (GAP43) (Verhaagen et al., 1989; Roskams et al., 1998). Terminal differentiation of canonical OSNs is marked by upregulation of ORs and olfactory marker protein (OMP) and is accompanied by migration from the more basal layers (where the GBCs are found) toward the apical surface of the OE (Miragall and Monti Graziadei, 1982; Rodriguez-Gil et al., 2015).

Like canonical OSNs, sensory neurons in the vomeronasal olfactory subsystem and the olfactory septal organ undergo renewal (Weiler and Farbman, 1997, 2003; Brann and Firestein, 2014). However, it remains unclear whether the primary sensory neurons of the GCD system, which are embedded within the main OE, are also renewed throughout the lifespan. GCD sensory neurons are densely packed in the caudal recesses of the OE (Fülle et al., 1995; Juilfs et al., 1997), a location that may protect these cells from the environmental insults that plague the more anterior regions of the main OE; the unusual location of most GCD OSNs, therefore, raises the possibility that adult GCD OSN renewal is slower (or even negligible) compared to that observed in the main system. Consistent with this possibility, neurons of the Grüneberg ganglion olfactory subsystem—which are unique in that they are encapsulated by a protective epithelial layer (Ma et al., 2015)—do not undergo adult neurogenesis (Fuss et al., 2005; Roppolo et al., 2006). To address this question, here we use 5-ethynyl-2'-deoxyuridine (EdU) labeling to ask whether GCD sensory neurons undergo renewal across the lifespan.

We find that GCD OSNs are continuously generated in juvenile and adult mice, with a subset of newly born neurons capable of long-term survival. After their final mitosis, GCD neurons serially express a number of marker proteins that, in the canonical OE and other neural cell types, are associated with progressively more differentiated fates. By taking advantage of these developmental markers, we demonstrate that the GCD precursors differentiate into mature neurons at similar timescales to canonical OSN precursors but that GCD OSNs exhibit unique patterns of marker expression and cell migration, which proceeds at least in part in a horizontal manner. These data demonstrate that—like canonical OSNs—GCD OSNs undergo continuous neurogenesis and establish a molecular and anatomical differentiation trajectory specific to adult-born GCD OSNs.

Materials and methods

Animals

Experiments on wild-type animals were performed on C57BL/6J mice of either sex obtained directly from the Jackson Laboratory (stock #000664). *Gucy2d-IRES-tauGFP* mice, in which cells express Tau-fused green fluorescent protein (GFP) under the control of the GCD gene *Gucy2d* (Hu et al., 2007), had been obtained from the Jackson Laboratory (stock #006704) and bred to homozygosity in-house. *Gucy2d*^{-/-} (GCD-null) mice (Leinders-Zufall et al., 2007) were a gift from Dr. Steven D. Munger and bred as homozygous nulls in-house. Mice were 6–9 weeks of age at the time of experiments unless they were injected with EdU, in which case ages at injection and sacrifice are indicated in main text and/or figure legends. Mice were group housed with up to 4 additional same-sex animals in plastic cages with cob bedding within a specific pathogen-free facility. Mice were maintained on 7 AM to 7 PM lights-off cycle; EdU injections and sacrifices were performed during the lights-off hours. All mouse husbandry and experiments were performed following institutional and federal guidelines and approved by the Institutional Animal Care and Use Committee at Harvard Medical School.

Mouse olfactory epithelium tissue preparation

After sacrifice, olfactory epithelia along with encapsulating bones and attached olfactory bulbs were rapidly excised and fixed in 4% formaldehyde (Electron Microscope Sciences, 19202) in 1× phosphate-buffered saline (PBS; VWR, 82021–502), pH 7.6, overnight at 4 °C. The following day, tissue was washed in PBS 3 times, then decalcified in 0.45-mM ethylenediaminetetraacetic acid in PBS overnight at 4 °C. Tissue was washed once more in PBS, equilibrated in 30% sucrose in PBS for at least 4 h at 4 °C, equilibrated in Tissue Freezing Medium (VWR, 15146-025) for at least 30 min, and then frozen on crushed dry ice. Frozen tissue was stored at –80 °C prior to being sectioned on a cryostat. Tissue sections 12- μ m thick were collected onto Superfrost Plus glass slides (VWR, 48311703) and stored at –80 °C until immunostaining. In order to capture most of the GCD OSNs, sections were collected from a 1.2–1.5-mm span of the main OE starting at its caudal tip that abuts the olfactory bulbs.

Immunostaining

All antibodies used are listed in Table 1. Slides containing tissue sections were retrieved from –80 °C and air-dried. Sections were permeabilized with 0.1% Triton X-100 in PBS for 15–30 min, then washed 3 times in PBS. TrueBlack Autofluorescence Quencher (Biotium, 23007) was then applied following protocol of the manufacturer to reduce OE background fluorescence in the green detection channel. Sections were then incubated for 30–60 min in blocking solution that consisted of PBS containing 3% bovine serum albumin (Jackson ImmunoResearch, 001-000-162) and 3% donkey serum (Jackson ImmunoResearch, 017-000-121), followed by overnight incubation at 4 °C with primary antibodies diluted in the same blocking solution. Following 3 washes in PBS, sections were incubated for 45 min with secondary antibodies diluted in blocking solution, washed again in PBS, and mounted with glass coverslips using Vectashield Mounting Medium (Vector Laboratories, H-1000). Nuclei were labeled by incubating tissue with 300-nM 4',6-diamidino-2-phenylindole (DAPI) in PBS for 10 min prior to mounting the coverslip. EdU development, when performed, followed TrueBlack treatment. All steps were performed at room temperature unless otherwise noted.

Table 1. Molecular reagents

Primary antibody	Source	Dilution
Rabbit α CART (polyclonal)	Phoenix Pharmaceuticals, H-003-62 (RRID: AB_2313614; see Dun et al. [2000] for validation by peptide competition)	1:2000
Mouse IgG1 α GAP43 (clone 91E12)	Millipore, MAB347 (RRID: AB_94881; antibody is standard in the field and labeling matches previous reports [Weiler and Benali, 2005])	1:200–1:1000
Rabbit α GCD (polyclonal)	Covance, custom antibody (see Greer et al. [2016] and Supplementary Figure S3 for details and validation in null mouse line)	1:500
Chicken α GFP (polyclonal)	Aves Labs, GFP-1010 (RRID: AB_2307313; antibody is standard in the field)	1:2000
Rat α KI67 (clone SOLA15)	ThermoFisher, 14-5698-82 (RRID: AB_10854564; see Sobecki et al. [2016] for validation in null mouse line)	1:100
Rabbit α MS4A6C (polyclonal)	Covance, custom antibody (see Greer et al. [2016] for details and validation by peptide competition)	1:500
Goat α OMP (polyclonal)	Wako Chemicals, 544–10001 (RRID: AB_2315007; see Baker et al. [1989] for validation by immunosorption)	1:5000
Mouse IgG1 α PAX6 (monoclonal)	Developmental Studies Hybridoma Bank, Pax6-supernatant (RRID: AB_528427; see Collinson et al. [2003] for validation in chimeric mouse line)	1:100
Goat α PDE2A (polyclonal)	Santa-Cruz, sc-17227 (RRID: AB_653928; see Baxendale and Fraser [2005] for validation by peptide competition)	1:100
Rabbit α PDE2A (polyclonal)	FabGenniX, PD2A-101AP (RRID: AB_2315082; see Liu et al. [2009] for validation by peptide competition)	1:500
Mouse IgG1 α PGP9.5 (monoclonal)	Abcam, ab72911 (RRID: AB_1269733; labeling matches previous reports [Weiler and Benali, 2005])	1:500
Mouse IgG2a α TUBB3 AF647 conjugate (clone TUJ1)	BioLegend, 801210 (RRID: AB_2686931; antibody is standard in the field and labeling matches previous reports for the same antigen [Roskams et al., 1998])	1:200
Secondary antibody	Source	Dilution
Donkey α Chicken AF488	Jackson ImmunoResearch, 703-545-155	1:300
Donkey α Goat AF488	Jackson ImmunoResearch, 705-546-147	1:300
Donkey α Goat Cy3	Jackson ImmunoResearch, 705-165-147	1:300
Donkey α Goat AF647	Jackson ImmunoResearch, 705-605-147	1:300
Goat α Mouse IgG1 AF555	Invitrogen, A21127	1:300
Goat α Mouse IgG1 AF647	Invitrogen, A21240	1:300
Donkey α Rabbit AF405	Abcam, ab175649	1:300
Donkey α Rabbit AF488	Abcam, ab150073	1:300
Donkey α Rabbit AF647	Jackson ImmunoResearch, 711-605-152	1:300
Goat α Rat AF633	Invitrogen, A21094	1:300
RNAscope target	Source	
<i>Cngb3</i>	Advanced Cell Diagnostics, 406161	

EdU cell proliferation assay

EdU (Invitrogen, A10044) was solubilized in sterile lactated Ringer's solution (Patterson Veterinary, 07-800-9333) to 10 mg/mL and injected intraperitoneally at 50 μ g per gram of body weight twice, 6 h apart. For day-of-injection sacrifice, tissue was harvested 2 h after the second injection. EdU was detected using Click-iT EdU Alexa Fluor 555 Imaging Kit (Invitrogen, C10338) following instructions of the manufacturer (manual MAN0002026, rev. 29 July 2011, MP10338).

RNAscope fluorescent in situ hybridization

Cngb3 transcript was detected by fluorescent RNAscope assay (Advanced Cell Diagnostics, kit 320851) using probe 406161

and Amp-4B following protocol of the manufacturer (*RNAscope Fluorescent Multiplex Kit User Manual*, 320293-UM Date 03142017; Wang et al., 2012). Prior to initiating the hybridization protocol, tissue was pretreated with 2 successive incubations—first 30 min, then 15 min long—in RNAscope Protease III (Advanced Cell Diagnostics, 322337) at 40 °C, then washed in distilled water. At the end of protocol, tissue was washed in PBS and subjected to the 2-day immunostaining protocol described in the immunofluorescence staining section, except the permeabilization step was omitted and ProLong Diamond Antifade Mountant (Invitrogen, P36961) was used in place of Vectashield. We observed that immunostaining steps reduced in situ signal intensity, but this attenuation did not influence our results.

Image acquisition

Confocal images were collected using Leica SPE microscope (Harvard Neurobiology Imaging Facility) using ACS APO 40X/1.15NA oil immersion objective at $\times 1.2$ – 1.5 optical zoom. At each field of view, a multichannel z-stack of 10–14 optical sections spaced 0.44–0.75 μm was collected. Excitation was performed sequentially using 405-, 488-, 561-, and 635-nm laser lines, and emission was detected using user-defined bandwidths. To create the OE schematic, epifluorescence images were acquired and stitched on Zeiss AxioScan Slide Scanner (Harvard Center for Biological Imaging) and accessed using ZEN software (Zeiss).

Image processing

Images used for scoring were not postprocessed; multislice z-stacks were used for manual identification and scoring of cells (see Analysis and quantification). Histology images are maximal intensity projections of multiple optical cross-sections spanning 3–7 μm in depth. Noisy images were median-smoothed using the *Remove Outliers* function built into Fiji image software (Schindelin et al., 2012). Occasional debris visible in the nasal cavity were masked.

Analysis and quantification

Images

Histology images of all initial scored samples were blinded with respect to mouse sex, age, and EdU chase period. To quantify the incidence of EdU incorporation or marker expression, cell bodies in a given image stack were manually identified according to the relevant inclusion marker (PDE2A⁺ or KI67⁺) and DAPI staining and then evaluated for the presence of EdU and/or marker colocalization. Only those cells were tallied in which the inclusion marker and DAPI-labeled nucleus were ascertained in multiple optical cross-sections, with 2 exceptions. First, as the samples evaluated for TUBB3 and CART coexpression in EdU-labeled GCD OSNs were not DAPI stained, for them, inclusion was based on the presence of EdU signal (which is nuclear). Second, to quantify marker expression in dendrites, scoring was done on PDE2A⁺ dendrites.

Cul-de-sac anatomy

To model cell locations, cul-de-sacs were individually fit with a parabola ($y = ax^2 + b$) so that the vertex mapped onto the inflection point of the cul-de-sac and the arms tracked neuronal layers of the arching sides. The center of the soma of each cell was annotated and associated with the nearest point on the respective parabola. The arc length of the parabola segment from the vertex to the projection point denotes the distance of that cell from cul-de-sac center. The “consensus” cul-de-sac in Figure 5A depicts raw coordinates of cells from 10 cul-de-sacs translated to common axes. Kernel density was estimated using the Seaborn package (Seaborn version 0.9.0, <https://seaborn.pydata.org>) in the Python programming language (Python Software Foundation, <https://www.python.org/>).

Statistics

The event of a cell being labeled by EdU (Figure 2D,E) or expressing GCD or MS4A6C (Figure 4C,D) was modeled by a Bernoulli trial. To compare labeled fractions across conditions, cell counts from animals belonging to a given condition were pooled and the resulting distributions were compared using Welch’s *t*-test using `stats.ttest_ind` function of the Scipy package (version 0.19.1) in Python. Fisher’s exact test yielded equivalent conclusions.

Results

Most GCD OSNs in adult rodents are found in clustered groups in the caudal regions of the OE (also referred to as the “cul-de-sac” regions or the “dorsal recesses” of the nasal cavity), although occasional GCD OSNs are distributed among canonical OSNs (Shinoda et al., 1989; Fülle et al., 1995; Juilfs et al., 1997; Greer et al., 2016). Although the anatomical location of GCD clusters in the OE has been previously mapped in neonatal rodents (Shinoda et al., 1989; Fülle et al., 1995), the spatial distribution of cul-de-sacs and isolated GCD OSNs has not been established in adult mice (but see Walz et al., 2007).

To identify GCD OSNs, we stained the OE with antibodies directed against phosphodiesterase 2A (PDE2A), which is expressed in all GCD OSNs (Juilfs et al., 1997; Meyer et al., 2000; Hu et al., 2007). PDE2A⁺ cells were identified in all turbinates of the adult OE at the stereotyped locations schematized in Figure 1A. Most of PDE2A⁺ clusters were localized to caudal recesses associated with the arching junctions of 2 turbinates or of a turbinate and outer bone or with the inner folds of a single turbinate; thus, most cul-de-sacs include both a curved compartment at the base and 2 straight compartments that are contiguous with the canonical epithelium (Figure 1B). We observed that the curved compartments were thinner than the straight ones (22–55 μm total or 2.8 ± 0.8 neuronal cell bodies thick for the curved compartments vs. 34–83 μm total or 5.8 ± 1.2 neuronal cell bodies for the straight compartments, range and mean \pm standard deviation, $n = 3$ mice). Within the cul-de-sacs, GCD OSNs form a discrete layer that is identifiable using the neural marker PGP9.5 (Figure 1B). We occasionally observe PDE2A⁺ microvillar cells that reside apically to the neuronal layer (data not shown; Hansen and Finger, 2008); these cells are ignored for the purposes of our analysis.

We also noted that GCD OSNs were organized into 2 types of anatomic clusters, which we designate type I and type II (Figure 1A,C). Type I clusters included dense concentrations of cells that expressed PDE2A at high levels and were rarely interspersed with identifiable canonical OSNs; these correspond to the canonical cul-de-sac regions that have been described previously (Fülle et al., 1995; Juilfs et al., 1997). Type II clusters were less common and contained fewer GCD OSNs that expressed low levels of PDE2A and were often intermingled with canonical OSNs. In addition, we occasionally observed solitary PDE2A-high GCD OSNs punctuating the canonical epithelium (Figure 1A,C). For consistency, in the remainder of this study, we focus on type I cell clusters, which we identify via PDE2A expression and anatomical location.

Proliferating basal cells are found within GCD cul-de-sacs

It is not yet established whether GCD OSNs—like canonical OSNs—are repopulated continuously throughout the lifespan. To address this question, we asked whether dividing cells could be identified within or near GCD cul-de-sacs by staining 6-week-old mice for KI67, a nuclear protein specific to all active phases of the cell cycle but absent in quiescent (G_0) cells. KI67⁺ nuclei were observed both within the straight and, less frequently, within the curved regions of GCD cul-de-sacs (Figure 2A–C, second column). Most of the KI67⁺ nuclei were close to the basal lamina that underlies the epithelium but were also occasionally observed in the apical layer of the canonical epithelium formed by sustentacular cells, as would be expected given the ongoing proliferation of this support cell population (Graziadei and Graziadei, 1979; Weiler and Farbman, 1998b).

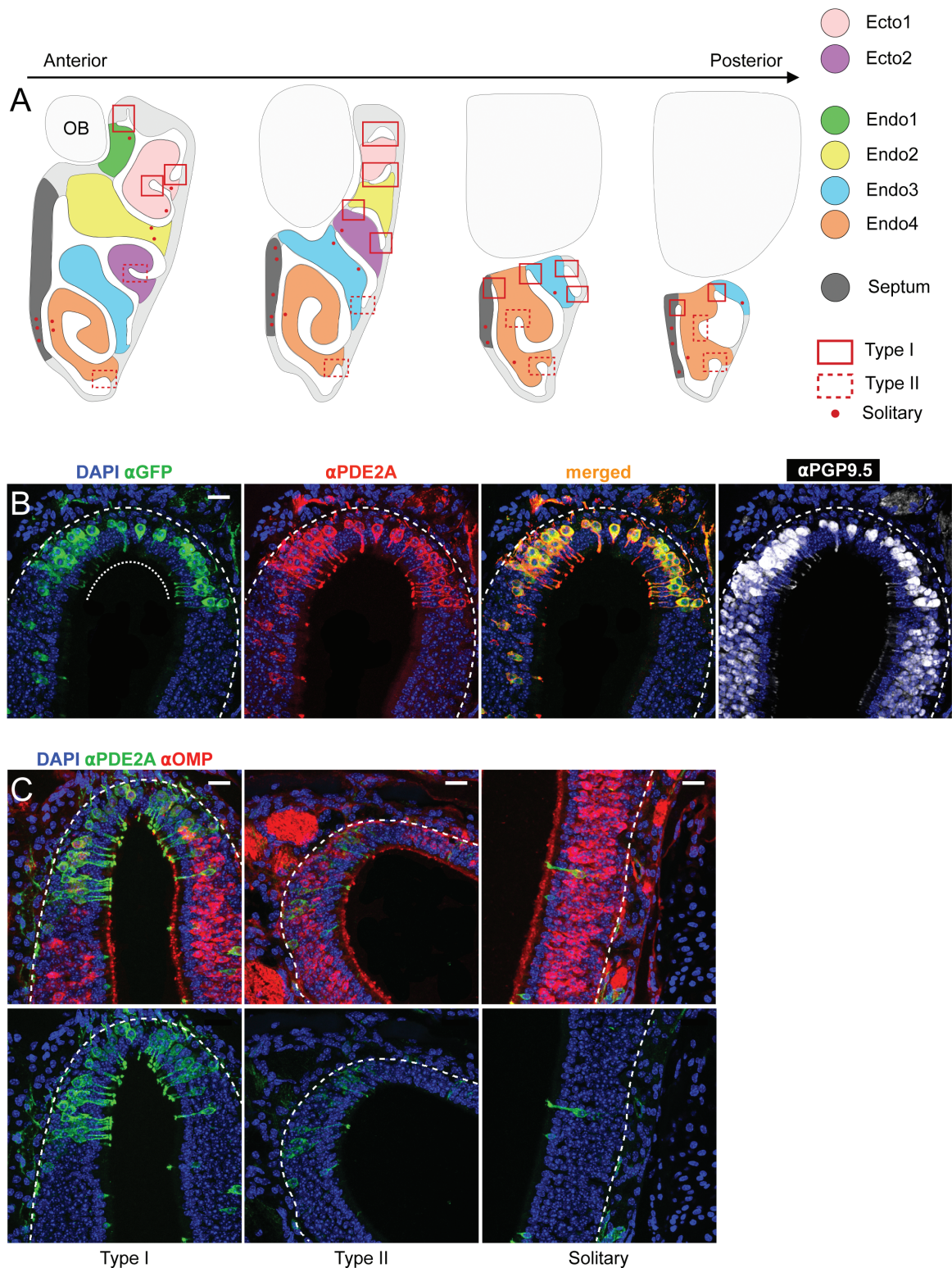


Figure 1. Stereotyped anatomical distribution of GCD OSNs in main OE. **(A)** Schematized localization of GCD cul-de-sacs and solitary GCD OSNs within coronal sections through the caudal OE with attached olfactory bulb (OB). Ethmoid turbinates are categorized as ectoturbinates (ecto) #1–2 (which are adjacent to the lateral wall of the epithelium) and endoturbinates (endo) #1–4 (which are either on the medial wall or internal to the epithelium) as has been done previously (Yang et al., 2018) and color-shaded, along with the septum, according to the legend. Type I clusters of GCD OSNs (solid outline; also see C, left) are prevalent in posterodorsal cul-de-sacs. Type II clusters of GCD OSNs (dotted outline; also see C, middle) are located more anteriorly and ventrally. Solitary GCD OSNs are dispersed but often found in stereotyped locations of the epithelium (dots; also see C, right) **(B)** In the *Gucy2d-IRES-tauGFP* mouse line (see Materials and methods), GCD-expressing OSNs coexpress GFP. OSNs identified with GFP (leftmost panel) are uniformly positive for PDE2A immunofluorescence (2 middle panels). Somas of GCD OSNs are localized to the neuronal layer that spans most of the OE, here identified by expression of neuronal marker PGP9.5 (rightmost panel). Curved region of the cul-de-sac is demarcated along the luminal surface with a fine dotted line. **(C)** Representative images of the 3 anatomical-molecular patterns exhibited by GCD OSNs. **(Left)** Type I GCD OSNs cluster. GCD OSNs often express low level of OMP, while canonical OE is defined by high level of OMP expression (red). **(Middle)** Type II GCD OSN cluster. **(Right)** Solitary GCD OSN embedded in canonical neuroepithelium. Basal lamina is delineated with dotted lines. Blue, DAPI. Scale bars, 20 μ m.

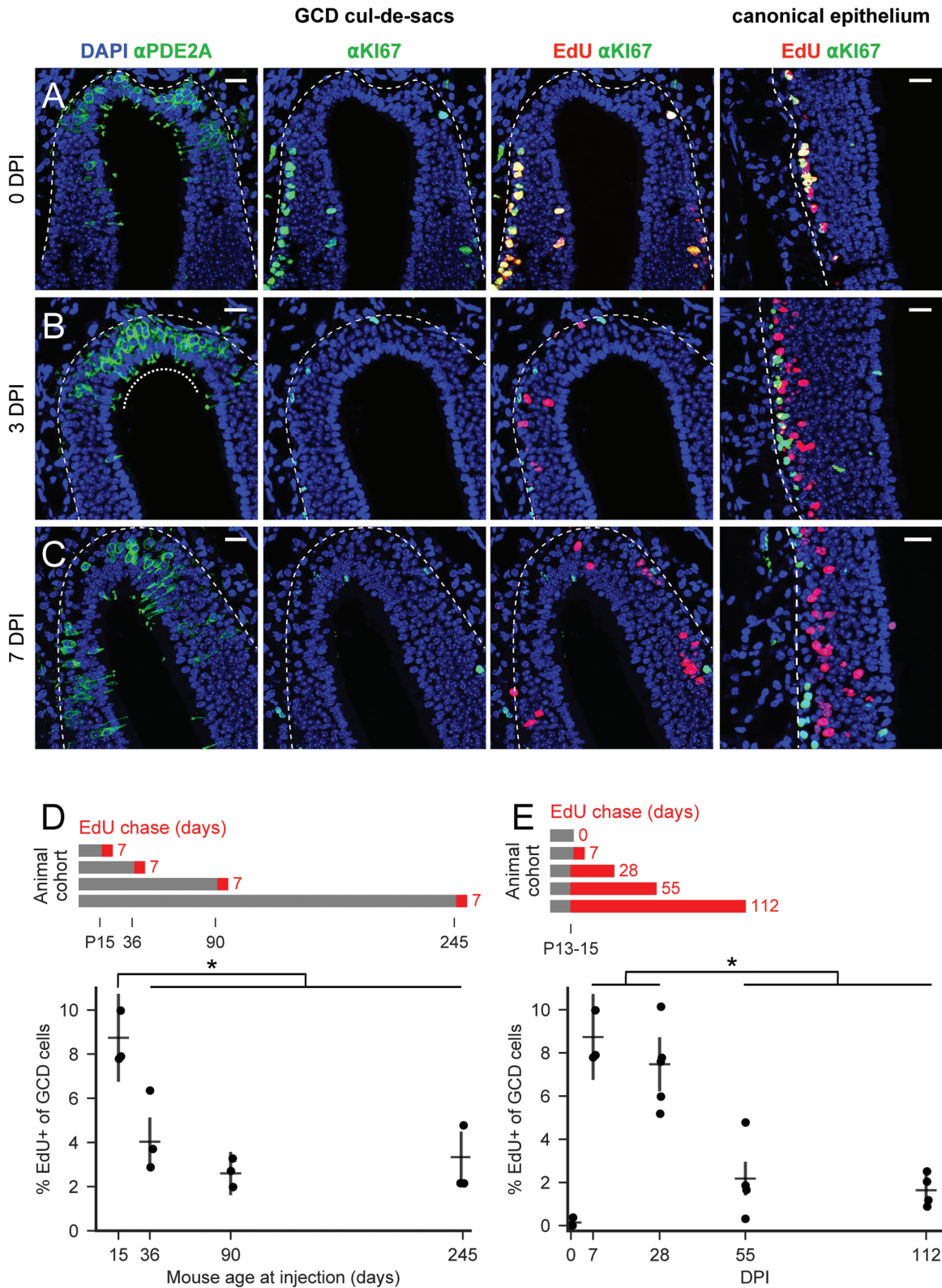


Figure 2. New GCD OSNs are born throughout adulthood and persist for months. **(A–C)** Expression of PDE2A and KI67 (green) and EdU localization (red) in sections of caudal OE of adult mice injected with EdU 0 **(A)**, 3 **(B)**, or 7 **(C)** days prior. Curved region of each cul-de-sac is demarcated along the luminal surface with a fine dotted line. Basal lamina is delineated with dotted lines. Blue, DAPI. Scale bars, 20 μ m. **(D, E; top)** Time course of EdU labeling associated with data in the bottom panels. Mice were EdU-injected on postnatal day indicated in black and sacrificed after the number of days indicated in red. **(D; bottom)** Percentage of EdU+ GCD OSNs after a 7-day chase in mice labeled at 15, 36, 90, or 245 days of age (3–5 mice per timepoint, >150 cells counted per mouse). For each age cohort, a cross shows the mean and 95% confidence interval after combining cell counts across mice. EdU+ fraction in mice labeled at P15 is statistically greater than that in mice labeled at older ages (1-sided Welch's *t*-test, $t = 5.21$, $P = 1E-7$), denoted by asterisk. **(E; bottom)** Similar to **(D)**, percentage of EdU+ GCD OSNs after different chase durations. Mice were EdU-labeled at P13–15 and sacrificed 0, 7, 28, 55, or 122 days later. EdU+ fraction in mice sacrificed at 7–28 DPI is statistically greater than in 55–122 DPI mice (1-sided Welch's *t*-test, $t = 9.65$, $P = 4E-22$), denoted by asterisk.

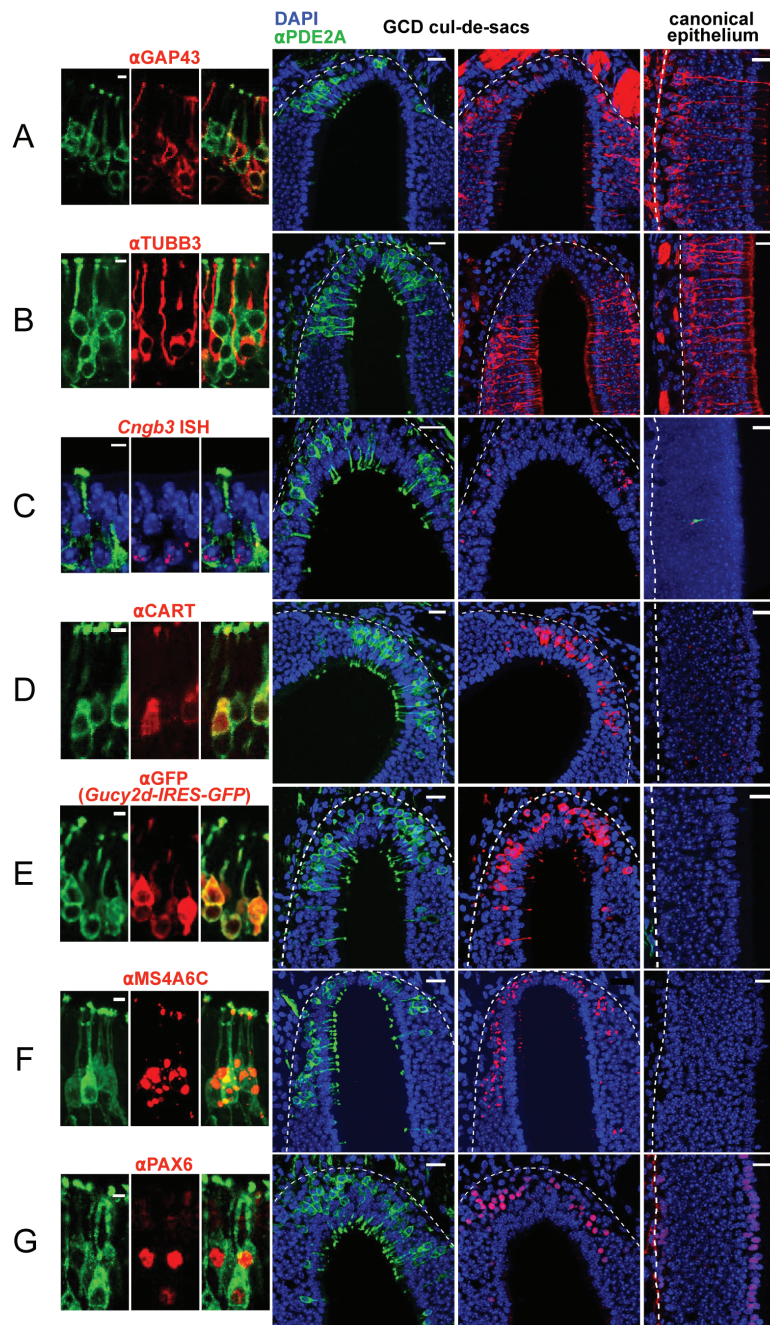


Figure 3. Differentiation and maturity markers are expressed heterogeneously in GCD OSNs. Representative images of marker expression in GCD OSNs (left and middle panels) and in canonical OSNs (right panels). Fraction of GCD OSNs expressing each marker, shown as mean \pm the standard error of the mean (SEM) across n mice: (A) GAP43 ($42 \pm 2\%$, $n = 8$), (B) TUBB3 ($19 \pm 4\%$, $n = 10$), (C) *Cngb3* ($69 \pm 2\%$, $n = 3$), (D) CART ($82 \pm 3\%$, $n = 10$), (E) GCD ($92 \pm 1\%$, $n = 5$), (F) MS4A6C ($91 \pm 3\%$, $n = 4$), and (G) PAX6 ($96 \pm 4\%$, $n = 3$). Expression was assayed by immunostaining for the target protein in wild-type tissue, except for *Cngb3* and GCD. *Cngb3* expression was assayed by RNAscope in situ hybridization (see Table 1) as CNGB3 protein was undetectable using commercial antibodies. Canonical OSNs were devoid of *Cngb3* transcript; here, we show an image that captures *Cngb3* expressed in a solitary PDE2A⁺ GCD OSN (C, right). Expression of GCD was inferred from GFP immunosignal in tissue from *Gucy2d-IRES-tauGFP* reporter mice (see Materials and methods). We obtained a similar GCD-expressing cell fraction ($95 \pm 1\%$, $n = 3$) when we quantified the expression of GCD protein in PDE2A⁺ dendritic knobs by immunostaining (Supplementary Figure S3). Note that nuclear PAX6 signal (G) was present in GCD OSNs, basal cells, and sustentacular cells but not in non-GCD OSNs. Red, target molecule; green, PDE2A; blue, DAPI. Basal lamina is delineated with dotted lines. Scale bars, 5 μ m in the left and 20 μ m in the 3 right columns.

KI67 signal never coincided with PDE2A, confirming that GCD OSNs are postmitotic.

Thus, KI67 staining revealed dividing progenitor cells within and adjacent to GCD cul-de-sac regions. To determine if GCD OSNs are derived from these cells, we pulsed cells with EdU and then tracked

patterns of marker expression over time. In mice sacrificed on the day of EdU injection, EdU signal largely overlapped with that for KI67 (Figure 2A and Supplementary Figure S1A), confirming that EdU was incorporated into dividing cells and that KI67 marked cycling cells. EdU⁺ cells were observed in the neuronal layer of the

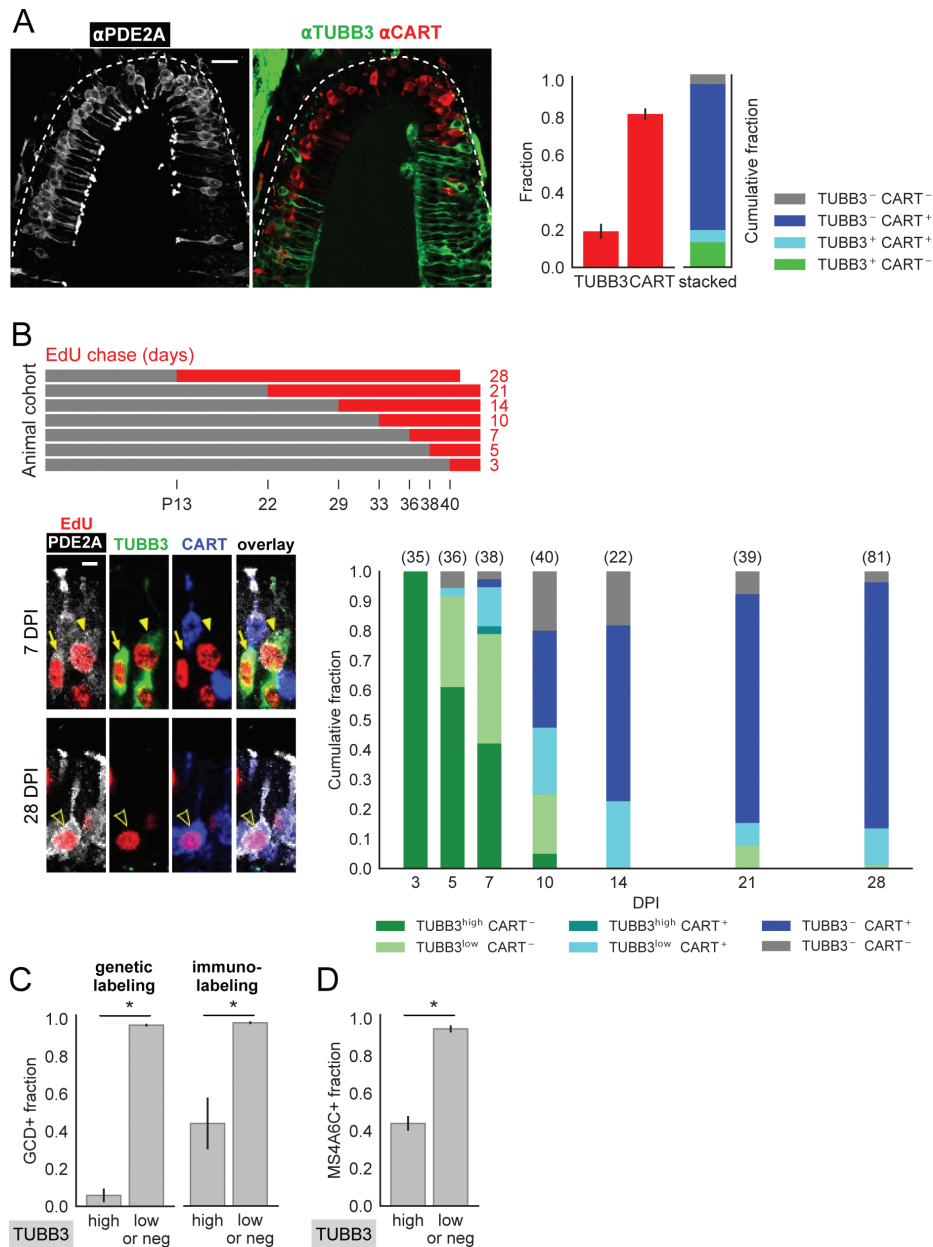


Figure 4. Expression of TUBB3, GCD, MS4A6C, and CART is temporally regulated in GCD OSNs. **(A)** TUBB3 and CART are expressed in complementary subsets of GCD OSNs. **(Left)** Triple immunofluorescence staining codetecting PDE2A (white), TUBB3 (green), and CART (red). Scale bar, 20 μ m. **(Right)** Red bars, fractions of GCD OSNs that express TUBB3 or CART (data from Figure 3B and D, respectively; error bars indicate SEM). Stacked bars, quantification of coexpression of TUBB3 and CART among GCD OSNs, shown as mean of each population across 10 mice: 95% expressed at least one of the markers, of which 6% coexpressed both; 13% and 76% expressed solely TUBB3 or CART, respectively. TUBB3⁺ CART⁻, TUBB3⁻ CART⁺, dual-positive, and dual-negative fractions of GCD OSNs are color-coded according to the legend. **(B)** Complementary expression of TUBB3 and CART during differentiation of GCD OSNs. **(Top)** Time course of EdU injections and chase periods associated with data in the bottom panel. Three mice were injected at each marked postnatal age and sacrificed at 41–43 days of age, resulting in EdU chase periods of 3, 5, 7, 10, 14, 21, and 28 days. **(Bottom; left)** Categorization of birthdated GCD OSNs according to TUBB3 and CART expression. EdU⁺ PDE2A⁺ neurons were scored as exhibiting high (TUBB3^{high}), low (TUBB3^{low}), or absence of TUBB3 signal, as well as for presence or absence of CART signal. TUBB3^{high} intensity was similar to that of basally located canonical OSNs, while TUBB3^{low} resembled that of apically located canonical OSNs. Three of the 6 possible GCD OSN phenotypes—TUBB3^{high} CART⁻ (filled arrow), TUBB3^{low} CART⁺ (filled arrowhead), and TUBB3⁻ CART⁺ (outlined arrowhead)—are shown in representative images from 7 and 28 DPI samples. The samples combine EdU detection (red) with immunostaining for PDE2A (white), TUBB3 (green), and CART (blue). Scale bar, 5 μ m. **(Bottom, right)** TUBB3/CART phenotypes, color-coded according to the legend, of EdU⁺ GCD OSNs at each chase period represented as fractions of all EdU⁺ GCD OSNs scored at that timepoint. Underlying cell counts, pooled from 3 mice per timepoint, are denoted in parentheses. **(C)** GCD expression in GCD OSNs correlates with level of TUBB3 expression. Two complementary approaches to quantifying coexpression reveal that TUBB3^{high} GCD OSNs express GCD at least 2-fold less frequently than do GCD OSNs with lower levels of TUBB3. **(Left)** GCD expression inferred from GFP immunosignal in tissue from *Gucy2d-IRES-tauGFP* reporter mice (6 \pm 4% in TUBB3^{high} vs. 97 \pm 1% in TUBB3^{low/negative} GCD OSNs, mean \pm SEM across 5 mice, plotted as bars and errors; 1-sided Welch's *t*-test on cell counts combined across animals, *t* = 24.7, *P* = 2E-29, denoted by asterisk). **(Right)** GCD immunosignal in dendritic knobs of wild-type mice (44 \pm 14% vs. 98 \pm 1%, mean \pm SEM across 3 mice; 1-sided Welch's *t*-test on cell counts combined across animals, *t* = 4.96, *P* = 2E-5, denoted by asterisk). **(D)** MS4A6C expression in GCD OSNs correlates with level of TUBB3 expression. Quantification of coexpression reveals that TUBB3^{high} GCD OSNs express MS4A6C 2-fold less frequently than do GCD OSNs with lower levels of TUBB3 (44 \pm 8% vs. 94 \pm 4%, mean \pm SEM across 4 mice; 1-sided Welch's *t*-test on cell counts combined across animals, *t* = 5.94, *P* = 6E-7, denoted by asterisk).

cul-de-sacs in noses harvested at 3 and 7 days post-EdU injection (DPI; Figure 2B,C), consistent with the possibility that cycling cells near the basal lamina give rise to progeny that differentiate into GCD OSNs. EdU⁺ cells in the canonical epithelium assessed at 0–7 DPI progressively migrated from basal to apical positions in the epithelium as did EdU⁺ cells in the straight regions of the cul-de-sacs (Figure 2A–C, right 2 columns). In contrast, EdU⁺ cells in the thinner, curved regions of the cul-de-sacs did not exhibit a clear pattern of laminar migration over time. These data suggest that the laminar pattern of cell migration typically observed during ongoing neurogenesis in the main epithelium may not apply to neuronal progenitors that live near or within the curved cul-de-sac regions.

New GCD OSNs are born throughout adulthood and persist for up to 4 months

To test whether newly generated cells in cul-de-sacs include GCD OSNs, we assessed whether EdU⁺ cells were also labeled with PDE2A. No overlap between EdU and PDE2A was observed at 0 DPI, but double-labeled cells with discernible apical and basal processes in the neuronal layer were observed at both 3 and 7 DPI (Supplementary Figure S2). PDE2A staining was stronger in the 7 DPI EdU-labeled GCD OSNs than in the 3 DPI cells (data not shown), suggesting that PDE2A expression ramps up starting ~3 days postmitosis. These observations demonstrate that new GCD OSNs are produced in adult animals.

To determine whether GCD neurogenesis occurs throughout the animal lifespan as is the case for canonical OSNs (Kondo et al., 2010; Brann and Firestein, 2014), mice aged 15, 36, 90, or 245 days were administered EdU and sacrificed after a 7-day chase period. Although EdU⁺ PDE2A⁺ neurons were present in all mice, the double-labeled GCD OSN fraction was largest (~9%) in animals injected on postnatal day (P) 15 (an age at which OE is still growing in size and neuron number; Gross et al., 1982; Suzuki and Takeda, 1993). The fraction of EdU-positive GCD OSN dropped 2–3-fold by P36 and remained constant at older mouse ages (Figure 2D). These data demonstrate that GCD birthrate drops sharply as mice complete postnatal development and enter adulthood but that GCD OSNs are continuously generated even in aged mice.

After acquiring their PDE2A⁺ fate, newly generated GCD OSNs could either be eliminated or persist for longer timescales. To assess the longevity of newly developed neurons in the GCD population, EdU was injected into P13–15 mice (the period of maximum neurogenesis) and noses were harvested either on the day of injection or after a 28-, 55-, or 112-day chase. As would be expected, GCD OSNs were free of EdU label on the day of injection. Relative to the ~9% EdU⁺ GCD OSNs observed at 7 DPI, the fraction of EdU⁺ PDE2A⁺ cells began to shrink by 28 DPI, leveled off to ~2% by 55 DPI, and was maintained at that level until at least 112 DPI (Figure 2E). These data suggest that the bulk of GCD OSNs generated at P15 are lost in the second month postmitosis but that ~20% of the cells that survive for 1 week persist for at least ~4 months.

EdU intercalates uniformly into the genome; thus, the EdU-positive cell population includes both the cells that have undergone division during the EdU pulse and cells that are the progeny of EdU⁺ cells. To verify that the EdU⁺ PDE2A⁺ cells we observe were generated during or shortly after the initial EdU pulse, KI67⁺ cycling cells within GCD cul-de-sacs were examined for EdU label retention after pulse termination. While, immediately after injection, nearly all the

KI67⁺ cells were EdU⁺, both 7 and 28 days after injection, less than 1% of KI67⁺ cells were EdU⁺ (Figure 2C and Supplementary Figure S1B). This result demonstrates that nearly all EdU⁺ cells had exited the cell cycle within 7 days of being labeled and is consistent with EdU⁺ PDE2A⁺ cells we observe in the GCD cul-de-sacs being the product of a terminal division.

Expression of markers and signaling cascade components in GCD OSNs is not uniform

Our data demonstrate that the GCD OSN population undergoes continuous renewal and, in adults, is composed of neurons that are between 3 days and several months of age. Thus, at the population level, there is significant heterogeneity in the age of GCD OSNs within the cul-de-sacs, raising the possibility that the youngest GCD OSNs have not yet fully differentiated into mature neurons. To test this hypothesis, we asked whether GCD OSNs express molecules associated in the canonical OE with neuronal growth and development. Canonical OSNs express high levels of GAP43 and the β -tubulin isoform TUBB3 for multiple days after birth or lesion-induced replacement but downregulate these molecules upon transitioning to a mature state (Verhaagen et al., 1989; Suzukawa et al., 2011). Consistent with previous reports, GAP43 signal was only present in basal, immature neurons in the canonical OE (Figure 3A). However, in contrast to a previous report suggesting lack of expression (Ring et al., 1997), immunostaining revealed GAP43 expression in the soma and processes of ~40% of GCD OSNs. As has been reported previously, among the canonical OSNs, TUBB3 signal was strong in the soma and processes of basal, immature neurons but weak in the cell bodies of more apical, mature neurons (Figure 3B; Lee and Pixley, 1994; Roskams et al., 1998). In contrast, TUBB3 immunostaining labeled ~20% of GCD OSNs, with negligible staining signal observed in the remainder of the cells. Importantly, nearly all TUBB3⁺ GCD OSNs were also GAP43⁺ (data not shown).

Consistent with the possibility that not all GCD OSNs are mature, only 70% of PDE2A⁺ OSNs expressed the RNA for CNGB3 (Figure 3C), a CNGA3-associated subunit required for odorant-induced depolarization of GCD OSNs (Matveev et al., 2008; Munger et al., 2010). Similarly, cocaine- and amphetamine-regulated transcript (CART) protein—which is expressed in mature neurons throughout the brain (Subhedar et al., 2014) and has been previously shown to specifically mark GCD OSNs (Huang et al., 2018)—was present in most (~80%) but not all GCD OSNs (Figure 3D). Expression of GCD itself, which has been used to define OSNs belonging to the GCD subsystem (Fülle et al., 1995; Hu et al., 2007; Walz et al., 2007), was also detected in most but not all PDE2A⁺ GCD OSNs (Figure 3E). Similarly, the MS4A receptor family member 6C, which, in the nose, is specific to GCD OSNs (Greer et al., 2016), was observed in ~90% GCD OSNs (Figure 3F). As a control, immunostaining revealed that the transcription factor PAX6 (which is only expressed in GCD OSNs amongst OE neurons; Guo et al., 2010; Parrilla et al., 2016) was observed in >95% of PDE2A⁺ cells (Figure 3G), suggesting that key aspects of neuronal identity are shared among the GCD OSNs, despite the observed heterogeneity in differentiation-related markers. Taken together, these findings demonstrate that the PDE2A⁺ neuronal population in the OE—which has been previously taken to be synonymous with the population of mature GCD OSNs—is comprised of heterogeneous cell states and raise the possibility that TUBB3 can be used to mark immature GCD OSNs and CART can be used to mark mature GCD OSNs.

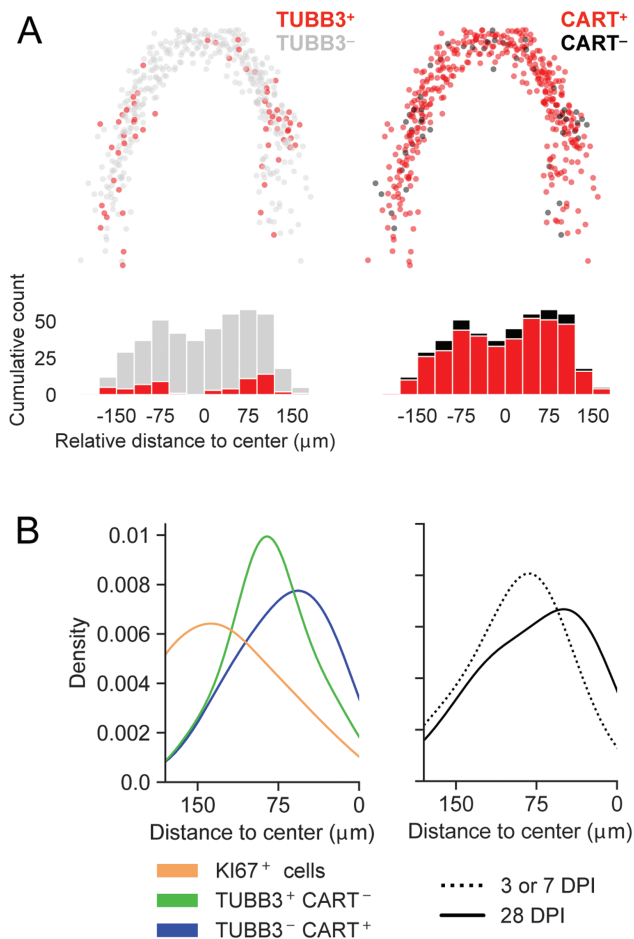


Figure 5. Location of GCD OSNs within a cul-de-sac correlates with state of differentiation. **(A)** Schematized locations of GCD OSNs within a consensus cul-de-sac created by overlaying positions of 447 cell bodies pooled from 10 images across different mice and imaging sites. Red circles represent GCD OSNs that express the target molecule, TUBB3 (left) or CART (right), while circles of contrasting color, gray (left) and black (right), represent GCD OSNs that do not. Histograms depict spatial distributions of these sets of neurons along the arching sides of the cul-de-sacs (see Materials and methods). Distance values of cells to the left of center are negative. **(B; Left)** Estimated density plots of absolute distance away from GCD cul-de-sac center of KI67⁺ cells ($n = 266$; beige), TUBB3⁺ CART⁻ GCD OSNs ($n = 31$; green) and TUBB3⁻ CART⁺ GCD OSNs ($n = 365$; blue). **(Right)** Analogous distribution estimates of EdU⁺ GCD OSNs at 3 or 7 DPI ($n = 39$; dotted line) versus 28 DPI ($n = 97$; solid line).

TUBB3 precedes expression of CART

If TUBB3 and CART mark immature and mature GCD OSNs, respectively, then TUBB3 and CART should label partially distinct populations of GCD OSNs. To test whether these markers demarcate distinct subsets of GCD population, the coexpression of TUBB3 and CART was examined in individual neurons. The vast majority (95%) of GCD OSNs expressed at least one of the 2 markers but only 6% expressed both, demonstrating that TUBB3 and CART expression does not substantially overlap (Figure 4A).

This observation—taken with prior work demonstrating that TUBB3 is an immaturity marker and CART marks mature cells in other types of neurons—suggests that TUBB3 is expressed in more immature GCD OSNs that transition into a CART-expressing phenotype as they develop. To directly test this hypothesis, mice were pulsed with EdU and noses were harvested between 3 and 28 days

postpulse (corresponding to the window of maximal EdU retention in GCD OSNs); noses were then triple immunostained against TUBB3, CART, and PDE2A to characterize the expression of TUBB3 and CART in EdU-birthdated GCD OSNs. At all timepoints, nearly all of the EdU-labeled GCD OSNs expressed TUBB3, CART, or both (Figure 4B). TUBB3 marked nearly all cells through 7 DPI, though its signal intensity was strongest at the earlier timepoints and waned across developmental time. The earliest CART-expressing GCD OSN, spotted at 5 DPI, was TUBB3^{low} as were nearly all of the more numerous CART⁺ neurons observed at the subsequent 7-day chase period. At 10 DPI, TUBB3 and CART each marked roughly half of birthdated GCD OSNs, yet only a small fraction expressed both. For chase periods of 2 weeks or longer, most cells were CART⁺ in the absence of TUBB3 and a small minority expressed both or neither of the molecules (Figure 4B).

These data demonstrate that TUBB3 expression both precedes and is anticorrelated with CART expression: TUBB3 declines with cellular age, while CART is upregulated. Moreover, the data indicate that TUBB3 offset and CART onset are temporally linked since both the double-positive and the double-negative fractions are small. In addition, these data reveal that GCD OSNs attain a stable TUBB3⁻/CART⁺ phenotype, at least at the population level, 2 weeks after labeling. Taken together, these observations suggest that TUBB3 and CART report progression through neuronal differentiation and mark the maturation state of GCD OSNs.

Expression of GCD and MS4A receptors occurs midway through GCD OSN maturation

In canonical OSNs, OR expression begins ~4 days after the final mitosis prior to downregulation of GAP43 and upregulation of OMP (Rodríguez-Gil et al., 2015). Mature GCD OSNs lack ORs but express GCD and MS4A receptors (Fülle et al., 1995; Juilfs et al., 1997; Greer et al., 2016). To map receptor expression onto the GCD differentiation timeline, we examined GCD OSNs in adult mice for coexpression of TUBB3 with GCD and MS4A6C.

Of TUBB3^{high} GCD OSNs (which we have established to be younger than 10 days of age; Figure 4B), a minority expressed GCD (Figure 4C). In contrast, of GCD OSNs that were TUBB3⁻ or TUBB3^{low}—which are at least 5 days of age but generally much older—nearly, all were GCD⁺. Similarly, only a minority of TUBB3^{high} but most of TUBB3⁻ or TUBB3^{low} GCD OSNs expressed MS4A6C (Figure 4D). These data indicate that over 90% of the older GCD OSNs express both GCD and MS4A receptors, confirming that the presence of both receptor types is a feature of mature GCD OSN identity (Greer et al., 2016).

These data demonstrate that GCD and MS4A expression follows PDE2A and—in a subset of GCD OSNs—precedes CART, with the remainder of GCD OSNs becoming receptor-positive as the cells lose TUBB3 and gain CART expression. Given that GCD and MS4A expression confers sensory responses upon GCD OSNs (Hu et al., 2007; Leinders-Zufall et al., 2007; Munger et al., 2010; Greer et al., 2016), these results are consistent with a model in which GCD OSNs undergo multiple stages of functional maturation after acquiring a PDE2A⁺ phenotype.

A lateralized progenitor pool populates GCD cul-de-sacs

We noted that the spatial distribution of TUBB3⁺ GCD OSNs was not uniform, with more TUBB3⁺ cells in the straight, more laminated arms and fewer in the central, curved region of the cul-de-sac (Figure 4A). Indeed, quantification of neuron distances to cul-de-sac

center showed that TUBB3⁺ GCD OSNs were infrequent inside the ~100- μ m-wide central curved region, while CART⁺ GCD OSNs did not exhibit the same anticenter bias (Figure 5A). This observation suggests a model in which the population of GCD cul-de-sacs arises from progenitor cells localized in the cul-de-sac arms and predicts that TUBB3⁺ GCD OSNs should be close to the dividing cells associated with each cul-de-sac. To investigate this, distances of KI67⁺ cells to cul-de-sac center were also quantified. Costaining for TUBB3 and CART revealed that the distributions of KI67⁺ cells, TUBB3⁺ CART⁻ GCD OSNs, and TUBB3⁻ CART⁺ GCD OSNs were each centered successively closer to cul-de-sac center; in other words, progenitors were farthest from the inflection in the cul-de-sac, young GCD OSNs were closer to the inflection, and older GCD OSNs were closer still (Figure 5B). Consistent with these findings, anatomical analysis of EdU label revealed that younger GCD OSNs were typically found further from cul-de-sac centers than 28-day-old GCD OSNs (Figure 5B). These findings demonstrate that cul-de-sac centers are populated, at least in part, via lateral migration and suggest that both marker expression—reflecting maturity—and anatomical location of a GCD OSNs within a cul-de-sac are governed by a common biological process.

Discussion

The main OE maintains progenitor pools that continually replace OR-expressing OSNs throughout the lifespan of a mouse. Here, we demonstrate that GCD OSNs also undergo continuous renewal. Differentiation of postmitotic GCD OSNs (identified by PDE2A immunoreactivity and location within the neuronal layer of the OE) is characterized by initial expression of established immaturity markers (GAP43 and TUBB3), followed by the onset of a marker of neural maturity (CART). While a subset of GCD OSNs express GCD and MS4A receptor proteins midway through maturation, most acquire a receptor-positive fate as CART expression becomes maximal. The switch from the immature to mature molecular phenotype takes ~10 days, on par with ~7 days required for newborn canonical OSNs to begin expressing OMP (Miragall and Monti Graziadei, 1982; Kondo et al., 2010; Savya et al., 2019). Anatomical mapping of marker expression and EdU label within GCD cul-de-sacs additionally suggests that a lateralized stem cell population drives the ongoing neurogenesis of GCD OSNs in the cul-de-sacs. These results reveal that GCD OSNs undergo continuous regeneration throughout the lifespan, define a developmental trajectory for those cells (Figure 6), and reveal a previously unappreciated heterogeneity amongst OSNs that are positive for PDE2A.

GCD OSNs renew but, on average, live less than 2 months

GCD OSNs born when the animal is 2 weeks old make up a stable fraction of the GCD OSNs population until the animal is 6 weeks of age, but this fraction decreases 3-fold over the month that follows; a similar trend is observed among canonical OSNs, where ~20% of neurons born at P10 and alive 1 week after go on to survive for 3 months (Kondo et al., 2010). The progressive decline over time in the fraction of GCD OSNs that were born in 2-week-old animals could be caused by either cell death or by an increase in the total number of GCD OSNs. The OE grows after birth but stabilizes in surface area by 7 weeks, around the same age that the number of GCD glomeruli reaches its adult count (Gross et al., 1982; Suzuki and Takeda, 1993; Walz et al., 2007). If, by extension, we assume

that the total number of GCD OSNs does not increase after this age, it is reasonable to infer that the drop in the fraction of EdU-labeled GCD OSNs observed at longer chase periods reflects ongoing cell death.

In addition, our data demonstrate that the rate of neurogenesis is significantly higher in younger mice when compared to older mice, although new GCD OSNs were observed in animals as old as 8 months. These findings—both of which are also true of canonical OSNs (Kondo et al., 2010)—suggest that long-lived GCD OSNs integrate into the GCD circuit and contribute to the function of the GCD olfactory subsystem.

A developmental trajectory for GCD OSNs

TUBB3 is a key component of neuronal cytoskeleton that is widely used as a marker of early neuronal development. In various tissues, including developing olfactory neurons, TUBB3 is expressed immediately before and during terminal mitosis (Menezes and Luskin, 1994; Memberg and Hall, 1995). As has been reported previously, we observe that, in the canonical OE, TUBB3 expression is high in developing neurons and is present but more modest in mature, more apical canonical OSNs (Lee and Pixley, 1994; Roskams et al., 1998). GCD OSNs also express high levels of TUBB3 early during the differentiation process, but expression of TUBB3 falls much more sharply over time in GCD OSNs when compared to canonical OSNs. Given the multiplicity of β -tubulin isoforms expressed in the mouse (of which TUBB3 is just one; Janke and Magiera, 2020) and the essential role played by β -tubulin in neural function, it is, therefore, likely that a β -tubulin other than TUBB3 is involved in microtubule maintenance in GCD OSNs.

We observe that CART expression rises as GCD OSNs mature, although the functional significance of this expression is not known. CART is a neuropeptide expressed in discrete peripheral sensory neural populations—for example, it selectively marks a set of functionally distinct retinal ganglion cells (Langer et al., 2018)—and widely distributed in the brain (Subhedar et al., 2014). Although a receptor for CART has not yet been identified, it is clear that CART peptides alter neural function and that, conversely, CART expression is influenced by internal states like fasting, stress, and hormonal status (Subhedar et al., 2014). Notably, expression of the GCD and MS4A receptors in GCD OSNs appears to coincide with the switch from TUBB3 to CART expression, suggesting that gaining a CART⁺ phenotype may be required for the full maturation of GCD OSNs; this observation is analogous to the canonical epithelium, where OR and OMP expression are key steps linked to the differentiation of OSN precursors into fully mature neurons (Sullivan et al., 1995; Lyons et al., 2013; Rodriguez-Gil et al., 2015).

Our data identify a small number of GCD OSNs that do not express either TUBB3 or CART. The fraction of double-negative cells among birthdated GCD OSNs varies with time postmitosis: while no double negatives are present early in neuronal development (3 days postdivision), they make up 20% of EdU-labeled GCD OSNs at 10 and 14 DPI and drop to the population average of 4–5% at 28 DPI. It is unclear how long the double-negative population persists past 28 DPI but, given the observed trends, it likely comprises an even smaller fraction of older GCD OSNs. The transient expansion of the double-negative population could reflect a simple lag in the onset of CART expression relative to TUBB3 downregulation or may capture GCD OSNs that failed to mature and are in the process of being eliminated from the population, akin to a subset of postnatally born canonical OSNs (Cowan and Roskams, 2002; Savya et al., 2019).

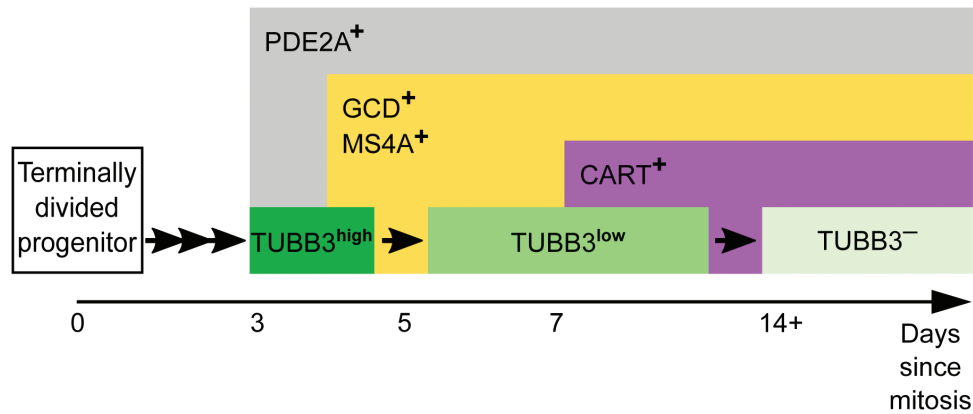


Figure 6. Proposed differentiation pathway of GCD OSNs. Molecular-temporal states of differentiation modeled on data in Figure 4. Onset of PDE2A expression is denoted by gray shading at 3 DPI, the earliest timepoint at which colocalization of PDE2A and EdU was observed. TUBB3 and CART expression profiles were established in EdU birthdating experiment. Onset of receptor expression (yellow shading) is based on data of GCD and MS4A6C colocalization with TUBB3^{high}.

Lateral migration of GCD OSNs during differentiation

In both the main OE and the vomeronasal sensory epithelium of the accessory olfactory system, neuroblast differentiation is coupled to ordered cell migration. In the OE, migration typically proceeds vertically with respect to the lumen. However, following chemical ablation of OE, neurons emanating from basal lamina neurogenic centers are thought to first migrate vertically, then laterally to fill in regions devoid of neurons (Roskams et al., 1998). Interestingly, under normal physiological circumstances, the vomeronasal epithelium contains 2 distinct neurogenic pools, one of which generates progeny that migrate vertically, while progeny of the other migrate laterally (Halpern and Martínez-Marcos, 2003; de la Rosa-Prieto et al., 2010). Among GCD OSNs present at the cul-de-sac centers, older (TUBB3⁻ CART⁺) OSNs are enriched relative to young (TUBB3⁺ CART⁻) OSNs. Furthermore, EdU⁺ PDE2A⁺ OSNs migrate over time from lateral positions to more central cul-de-sac locations. These observations suggest that some GCD OSNs populate cul-de-sac centers through an “outside-in” form of lateral migration and predict that senescent cell death will be maximal in the cul-de-sac centers that house the oldest GCD OSNs.

Progenitor cells for the GCD system

Our findings indicate that a set of mitotic progenitors in GCD cul-de-sacs are capable of differentiating into PDE2A⁺ GCD OSNs. Although, in this study, we do not identify these progenitor cells or their immediate progeny, given the anatomical proximity of the edges of the cul-de-sacs and the canonical epithelium, as well as the occasional presence of canonical OSNs within GCD cul-de-sacs, our data raise the possibility that GCD and canonical OSNs share a common progenitor pool (Fletcher et al., 2017; Schwob et al., 2017). Consistent with this possibility, GBCs can differentiate into either canonical OSNs or OSNs belonging to the trace amine-associated receptors system (Johnson et al., 2012) and give rise to neurons whose molecular fates are appropriate to their position along the dorso-ventral axis of the epithelium after transplantation (Chen et al., 2004; Coleman et al., 2019).

Alternatively, GCD OSNs may arise from a dedicated progenitor pool distinct from that used to populate the canonical epithelium. There is evidence that, during embryogenesis, GCD cul-de-sac regions exhibit higher rates of proliferation than the rest of the OE

and PDE2A⁺ OSNs emerge later than canonical OSNs (Yang et al., 2018). These observations suggest that neuronal progenitors in the OE may become specialized for production of GCD OSNs at later stages of development, perhaps due to the influence of location-specific determinants. Future work will be required to clarify whether GCD and canonical OSNs arise from a shared or distinct progenitor population.

Supplementary material

Supplementary material can be found at *Chemical Senses* online.

Acknowledgments

RNAscope experiments were performed with assistance from the Harvard Neurobiology Imaging Facility core. We thank the Harvard Center for Biological Imaging for infrastructure and support. We thank Slater Sharp for providing *Gucy2d-IRE5-tauGFP* mice, Tatsuya Tsukahara for insightful feedback, and all members of the Datta lab for helpful discussions and comments. We thank Neha Bhagat, Veronica Nikolaki, Tatsuya Tsukahara, Stan Pashkovski, and Slater Sharp for laboratory assistance.

Funding

S.R.D. is supported by National Institutes of Health grants RO1DC016222 and U19NS112953 and by the Simons Collaboration on the Global Brain. Imaging experiments were supported by the National Institute of Neurological Disorders and Stroke P30 Core Center Grant NS072030 (Harvard Neurobiology Imaging Facility).

Conflicts of interests

No conflicts of interest to report.

References

- Ajmani GS, Suh HH, Pinto JM. 2016. Effects of ambient air pollution exposure on olfaction: a review. *Environ Health Perspect.* 124(11):1683–1693.
- Arakawa H, Kelliher KR, Zufall F, Munger SD. 2013. The receptor guanylyl cyclase type D (GC-D) ligand uroguanylin promotes the acquisition of food preferences in mice. *Chem Senses.* 38(5):391–397.
- Axel R. 1995. The molecular logic of smell. *Sci Am.* 273(4):154–159.
- Baker H, Grillo M, Margolis FL. 1989. Biochemical and immunocytochemical characterization of olfactory marker protein in the rodent central nervous system. *J Comp Neurol.* 285(2):246–261.

- Baxendale RW, Fraser LR. 2005. Mammalian sperm phosphodiesterases and their involvement in receptor-mediated cell signaling important for capacitation. *Mol Reprod Dev.* 71(4):495–508.
- Brann JH, Firestein SJ. 2014. A lifetime of neurogenesis in the olfactory system. *Front Neurosci.* 8:182.
- Brook I. 2011. Microbiology of sinusitis. *Proc Am Thorac Soc.* 8(1):90–100.
- Chen X, Fang H, Schwob JE. 2004. Multipotency of purified, transplanted globe basal cells in olfactory epithelium. *J Comp Neurol.* 469(4):457–474.
- Coleman JH, Lin B, Louie JD, Peterson J, Lane RP, Schwob JE. 2019. Spatial determination of neuronal diversification in the olfactory epithelium. *J Neurosci.* 39(5):814–832.
- Collinson JM, Quinn JC, Hill RE, West JD. 2003. The roles of Pax6 in the cornea, retina, and olfactory epithelium of the developing mouse embryo. *Dev Biol.* 255(2):303–312.
- Cowan CM, Roskams AJ. 2002. Apoptosis in the mature and developing olfactory neuroepithelium. *Microsc Res Tech.* 58(3):204–215.
- de la Rosa-Prieto C, Saiz-Sanchez D, Ubeda-Bañon I, Argandoña-Palacios L, García-Muñozguren S, Martínez-Marcos A. 2010. Neurogenesis in subclasses of vomeronasal sensory neurons in adult mice. *Dev Neurobiol.* 70:961–970.
- DeMaria S, Ngai J. 2010. The cell biology of smell. *J Cell Biol.* 191(3):443–452.
- Dun NJ, Dun SL, Kwok EH, Yang J, Chang J. 2000. Cocaine- and amphetamine-regulated transcript-immunoreactivity in the rat sympatho-adrenal axis. *Neurosci Lett.* 283(2):97–100.
- Fletcher RB, Das D, Gadye L, Street KN, Baudhuin A, Wagner A, Cole MB, Flores Q, Choi YG, Yosef N, et al. 2017. Deconstructing olfactory stem cell trajectories at single-cell resolution. *Cell Stem Cell.* 20(6):817–830.e8.
- Fülle HJ, Vassar R, Foster DC, Yang RB, Axel R, Garbers DL. 1995. A receptor guanylyl cyclase expressed specifically in olfactory sensory neurons. *Proc Natl Acad Sci USA.* 92(8):3571–3575.
- Fuss SH, Omura M, Mombaerts P. 2005. The Grueneberg ganglion of the mouse projects axons to glomeruli in the olfactory bulb. *Eur J Neurosci.* 22(10):2649–2654.
- Gao L, Hu J, Zhong C, Luo M. 2010. Integration of CO₂ and odorant signals in the mouse olfactory bulb. *Neuroscience.* 170(3):881–892.
- Graziadei PP, Graziadei GA. 1979. Neurogenesis and neuron regeneration in the olfactory system of mammals. I. Morphological aspects of differentiation and structural organization of the olfactory sensory neurons. *J Neurocytol.* 8(1):1–18.
- Greer PL, Bear DM, Lassance JM, Bloom ML, Tsukahara T, Pashkovski SL, Masuda FK, Nowlan AC, Kirchner R, Hoekstra HE, et al. 2016. A family of non-GPCR chemosensors defines an alternative logic for mammalian olfaction. *Cell.* 165(7):1734–1748.
- Gross EA, Swenberg JA, Fields S, Popp JA. 1982. Comparative morphometry of the nasal cavity in rats and mice. *J Anat.* 135(Pt 1):83–88.
- Guo Z, Packard A, Krolewski RC, Harris MT, Manglapus GL, Schwob JE. 2010. Expression of pax6 and sox2 in adult olfactory epithelium. *J Comp Neurol.* 518(21):4395–4418.
- Halpern M, Martínez-Marcos A. 2003. Structure and function of the vomeronasal system: an update. *Prog Neurobiol.* 70(3):245–318.
- Hansen A, Finger TE. 2008. Is TrpM5 a reliable marker for chemosensory cells? Multiple types of microvillous cells in the main olfactory epithelium of mice. *BMC Neurosci.* 9:115.
- Hinds JW, Hinds PL, McNelly NA. 1984. An autoradiographic study of the mouse olfactory epithelium: evidence for long-lived receptors. *Anat Rec.* 210(2):375–383.
- Hu J, Zhong C, Ding C, Chi Q, Walz A, Mombaerts P, Matsunami H, Luo M. 2007. Detection of near-atmospheric concentrations of CO₂ by an olfactory subsystem in the mouse. *Science.* 317(5840):953–957.
- Huang Z, Zimmerman AD, Munger SD. 2018. Unique molecular markers for GC-D-expressing olfactory sensory neurons and chemosensory neurons of the Grueneberg ganglion. doi: [10.1101/346502](https://doi.org/10.1101/346502).
- Imamura F, Hasegawa-Ishii S. 2016. Environmental toxicants-induced immune responses in the olfactory mucosa. *Front Immunol.* 7:475.
- Janke C, Magiera MM. 2020. The tubulin code and its role in controlling microtubule properties and functions. *Nat Rev Mol Cell Biol.* doi: [10.1038/s41580-020-0214-3](https://doi.org/10.1038/s41580-020-0214-3).
- Johnson MA, Tsai L, Roy DS, Valenzuela DH, Mosley C, Magklara A, Lomvardas S, Liberles SD, Barnea G. 2012. Neurons expressing trace amine-associated receptors project to discrete glomeruli and constitute an olfactory subsystem. *Proc Natl Acad Sci USA.* 109(33):13410–13415.
- Juilfs DM, Fülle HJ, Zhao AZ, Houslay MD, Garbers DL, Beavo JA. 1997. A subset of olfactory neurons that selectively express cGMP-stimulated phosphodiesterase (PDE2) and guanylyl cyclase-D define a unique olfactory signal transduction pathway. *Proc Natl Acad Sci USA.* 94(7):3388–3395.
- Kondo K, Suzukawa K, Sakamoto T, Watanabe K, Kanaya K, Ushio M, Yamaguchi T, Nibu K, Kaga K, Yamasoba T. 2010. Age-related changes in cell dynamics of the postnatal mouse olfactory neuroepithelium: cell proliferation, neuronal differentiation, and cell death. *J Comp Neurol.* 518(11):1962–1975.
- Kondo K, Watanabe K, Sakamoto T, Suzukawa K, Nibu K, Kaga K, Yamasoba T. 2009. Distribution and severity of spontaneous lesions in the neuroepithelium and Bowman's glands in mouse olfactory mucosa: age-related progression. *Cell Tissue Res.* 335(3):489–503.
- Langer KB, Ohlemacher SK, Phillips MJ, Fligor CM, Jiang P, Gamm DM, Meyer JS. 2018. Retinal ganglion cell diversity and subtype specification from human pluripotent stem cells. *Stem Cell Rep.* 10(4):1282–1293.
- Lee VM, Pixley SK. 1994. Age and differentiation-related differences in neuron-specific tubulin immunostaining of olfactory sensory neurons. *Brain Res Dev Brain Res.* 83(2):209–215.
- Leinders-Zufall T, Cockerham RE, Michalakakis S, Biel M, Garbers DL, Reed RR, Zufall F, Munger SD. 2007. Contribution of the receptor guanylyl cyclase GC-D to chemosensory function in the olfactory epithelium. *Proc Natl Acad Sci USA.* 104(36):14507–14512.
- Liberles SD. 2015. Trace amine-associated receptors: ligands, neural circuits, and behaviors. *Curr Opin Neurobiol.* 34:1–7.
- Lin W, Arellano J, Slotnick B, Restrepo D. 2004. Odors detected by mice deficient in cyclic nucleotide-gated channel subunit A2 stimulate the main olfactory system. *J Neurosci.* 24(14):3703–3710.
- Liu CY, Fraser SE, Koos DS. 2009. Grueneberg ganglion olfactory subsystem employs a cGMP signaling pathway. *J Comp Neurol.* 516(1):36–48.
- Luo M. 2008. The necklace olfactory system in mammals. *J Neurogenet.* 22(3):229–238.
- Lyons DB, Allen WE, Goh T, Tsai L, Barnea G, Lomvardas S. 2013. An epigenetic trap stabilizes singular olfactory receptor expression. *Cell.* 154(2):325–336.
- Ma M, Fleischer J, Breer H, Eisthen H. 2015. The septal organ, grueneberg ganglion, and terminal nerve. In: Doty RL, editor. *Handbook of olfaction and gestation*. Hoboken (NJ): John Wiley & Sons, Inc. p. 1133–1150.
- Matveev AV, Quiambao AB, Browning Fitzgerald J, Ding XQ. 2008. Native cone photoreceptor cyclic nucleotide-gated channel is a heterotetrameric complex comprising both CNGA3 and CNGB3: a study using the cone-dominant retina of Nrl^{-/-} mice. *J Neurochem.* 106(5):2042–2055.
- Memberg SP, Hall AK. 1995. Dividing neuron precursors express neuron-specific tubulin. *J Neurobiol.* 27(1):26–43.
- Menezes JR, Luskin MB. 1994. Expression of neuron-specific tubulin defines a novel population in the proliferative layers of the developing telencephalon. *J Neurosci.* 14(9):5399–5416.
- Meyer MR, Angele A, Kremmer E, Kaupp UB, Muller F. 2000. A cGMP-signaling pathway in a subset of olfactory sensory neurons. *Proc Natl Acad Sci USA.* 97(19):10595–10600.
- Miragall F, Monti Graziadei GA. 1982. Experimental studies on the olfactory marker protein. II. Appearance of the olfactory marker protein during differentiation of the olfactory sensory neurons of mouse: an immunohistochemical and autoradiographic study. *Brain Res.* 239(1):245–250.
- Mohrhardt J, Nagel M, Fleck D, Ben-Shaul Y, Spehr M. 2018. Signal detection and coding in the accessory olfactory system. *Chem Senses.* 43(9):667–695.
- Munger SD. 2009. Olfaction: noses within noses. *Nature.* 459(7246):521–522.
- Munger SD, Leinders-Zufall T, McDougall LM, Cockerham RE, Schmid A, Wandernoth P, Wennemuth G, Biel M, Zufall F, Kelliher KR. 2010. An olfactory subsystem that detects carbon disulfide and mediates food-related social learning. *Curr Biol.* 20(16):1438–1444.

- Parrilla M, Chang I, Degl'Innocenti A, Omura M. 2016. Expression of homeobox genes in the mouse olfactory epithelium. *J Comp Neurol*. 524(14):2713–2739.
- Ring G, Mezza RC, Schwob JE. 1997. Immunohistochemical identification of discrete subsets of rat olfactory neurons and the glomeruli that they innervate. *J Comp Neurol*. 388(3):415–434.
- Rodriguez-Gil DJ, Bartel DL, Jaspers AW, Mobley AS, Imamura F, Greer CA. 2015. Odorant receptors regulate the final glomerular coalescence of olfactory sensory neuron axons. *Proc Natl Acad Sci USA*. 112(18):5821–5826.
- Roppolo D, Ribaud V, Jungo VP, Lüscher C, Rodriguez I. 2006. Projection of the Grüneberg ganglion to the mouse olfactory bulb. *Eur J Neurosci*. 23(11):2887–2894.
- Roskams AJ, Cai X, Ronnett GV. 1998. Expression of neuron-specific beta-III tubulin during olfactory neurogenesis in the embryonic and adult rat. *Neuroscience*. 83(1):191–200.
- Savya SP, Kunkhyen T, Cheetham CEJ. 2019. Low survival rate of young adult-born olfactory sensory neurons in the undamaged mouse olfactory epithelium. *J Bioenerg Biomembr*. 51(1):41–51.
- Schindelin J, Arganda-Carreras I, Frise E, Kaynig V, Longair M, Pietzsch T, Preibisch S, Rueden C, Saalfeld S, Schmid B, et al. 2012. Fiji: an open-source platform for biological-image analysis. *Nat Methods*. 9(7):676–682.
- Schwob JE, Jang W, Holbrook EH, Lin B, Herrick DB, Peterson JN, Hewitt Coleman J. 2017. Stem and progenitor cells of the mammalian olfactory epithelium: taking poetic license. *J Comp Neurol*. 525(4):1034–1054.
- Seiden AM. 2004. Postviral olfactory loss. *Otolaryngol Clin North Am*. 37(6):1159–1166.
- Shinoda K, Shiotani Y, Osawa Y. 1989. “Necklace olfactory glomeruli” form unique components of the rat primary olfactory system. *J Comp Neurol*. 284(3):362–373.
- Sobecki M, Mrouj K, Camasses A, Parisis N, Nicolas E, Llères D, Gerbe F, Prieto S, Krasinska L, David A, et al. 2016. The cell proliferation antigen Ki-67 organises heterochromatin. *Elife*. 5:e13722.
- Sokpor G, Abbas E, Rosenbusch J, Staiger JF, Tuoc T. 2018. Transcriptional and epigenetic control of mammalian olfactory epithelium development. *Mol Neurobiol*. 55(11):8306–8327.
- Subbendar NK, Nakhate KT, Upadhya MA, Kokare DM. 2014. CART in the brain of vertebrates: circuits, functions and evolution. *Peptides*. 54:108–130.
- Sullivan SL, Bohm S, Ressler KJ, Horowitz LF, Buck LB. 1995. Target-independent pattern specification in the olfactory epithelium. *Neuron*. 15(4):779–789.
- Suzukawa K, Kondo K, Kanaya K, Sakamoto T, Watanabe K, Ushio M, Kaga K, Yamasoba T. 2011. Age-related changes of the regeneration mode in the mouse peripheral olfactory system following olfactotoxic drug methimazole-induced damage. *J Comp Neurol*. 519(11):2154–2174.
- Suzuki Y, Takeda M. 1993. Basal cells in the mouse olfactory epithelium during development: immunohistochemical and electron-microscopic studies. *Brain Res Dev Brain Res*. 73(1):107–113.
- Uchida N, Poo C, Haddad R. 2014. Coding and transformations in the olfactory system. *Annu Rev Neurosci*. 37:363–385.
- Vent J, Robinson AM, Gentry-Nielsen MJ, Conley DB, Hallworth R, Leopold DA, Kern RC. 2004. Pathology of the olfactory epithelium: smoking and ethanol exposure. *Laryngoscope*. 114(8):1383–1388.
- Verhaagen J, Oestreicher AB, Gispens WH, Margolis FL. 1989. The expression of the growth associated protein B50/GAP43 in the olfactory system of neonatal and adult rats. *J Neurosci*. 9(2):683–691.
- Walz A, Feinstein P, Khan M, Mombaerts P. 2007. Axonal wiring of guanylate cyclase-D-expressing olfactory neurons is dependent on neuropilin 2 and semaphorin 3F. *Development*. 134(22):4063–4072.
- Wang F, Flanagan J, Su N, Wang LC, Bui S, Nielson A, Wu X, Vo HT, Ma XJ, Luo Y. 2012. RNAscope: a novel in situ RNA analysis platform for formalin-fixed, paraffin-embedded tissues. *J Mol Diagn*. 14(1):22–29.
- Weiler E, Benali A. 2005. Olfactory epithelia differentially express neuronal markers. *J Neurocytol*. 34(3–5):217–240.
- Weiler E, Farbman AI. 1997. Proliferation in the rat olfactory epithelium: age-dependent changes. *J Neurosci*. 17(10):3610–3622.
- Weiler E, Farbman AI. 1998a. Proliferation decrease in the olfactory epithelium during postnatal development. *Ann NY Acad Sci*. 855:230–234.
- Weiler E, Farbman AI. 1998b. Supporting cell proliferation in the olfactory epithelium decreases postnatally. *Glia*. 22(4):315–328.
- Weiler E, Farbman AI. 2003. The septal organ of the rat during postnatal development. *Chem Senses*. 28(7):581–593.
- Yang LM, Huh SH, Ornitz DM. 2018. FGF20-expressing, wnt-responsive olfactory epithelial progenitors regulate underlying turbinate growth to optimize surface area. *Dev Cell*. 46(5):564–580.e5.